Volume 12, Issue 3, Page 52-59, 2023 https://doi.org/10.46810/tdfd.1266393 Research Article

BİNGÖL ÜNİVERSİTESİ

Türk Doğa ve Fen Dergisi
Turkish Journal of Nature and Science

www.dergipark.gov.tr/tdfd

# Comparison of Different Supervised Classification Algorithms for Mapping Paddy Rice Areas Using Landsat 9 Imageries

**Melis INALPULAT**[1,2*]

[1] Çanakkale Onsekiz Mart University, Faculty of Agriculture, Department of Agricultural Structures and Irrigation, Agricultural Remote Sensing Laboratory (AGRESEL), Çanakkale, Türkiye
[2] Çanakkale Onsekiz Mart University, Computer-Agriculture-Environment-Planning (ComAgEnPlan) Study Group, Çanakkale, Türkiye
Melis INALPULAT ORCID No: 0000-0001-7418-1666

**Corresponding author: melissacan@comu.edu.tr*

(Received: 16.03.2023, Accepted: 7.08.2023, Online Publication: 27.09.2023)

**Keywords**
Çanakkale, Landsat 9, Paddy rice, Performance comparison, Supervised classification algorithms

**Abstract:** Rice is known to be one of the most essential crops in Türkiye, as well as many other countries especially in Asia, whereas paddy rice cropping systems have a key role in many processes ranging from human nutrition to environment-related perspectives. Therefore, determination of cultivation area is still a hot topic among researchers from various disciplines, planners, and decision makers. In present study, it was aimed to evaluate performances of three classifications algorithms among most widely used ones, namely, maximum likelihood (ML), random forest (RF), and k-nearest neighborhood (KNN), for paddy rice mapping in a mixed cultivation area located in Biga District of Çanakkale Province, Türkiye. Visual, near-infrared, and shortwave-infrared bands of Landsat 9 acquired on July 04, 2022 was utilized. The classification scheme included six classes as dense vegetation (D), sparse vegetation (S), agricultural field (A), water surface (W), residential area – base soil (RB), and paddy rice (PR). The performances were tested using the same training samples and accuracy control points. The reliability of each classification was evaluated through accuracy assessments considering 150 equalized randomized control points. Accordingly, RF algorithm could identify PR areas with over 96.0% accuracy, and it was followed by KNN with 92.0%. Using one-date Landsat 9 imagery seemed to have potential for PR area determination at high accuracy levels. In conclusion, RF algorithm is strongly suggested for reliable distinction of PR areas from neighbor classes under similar climate, soil and terrain conditions with comparable cultivation patterns, whereas Landsat 9 presents valuable data set for similar studies by being free of charge.



# Landsat 9 Kullanılarak Çeltik Alanlarının Haritalanması için Farklı Kontrollü Sınıflandırma Algoritmalarının Karşılaştırılması

**Anahtar Kelimeler**
Çanakkale, Landsat 9, Çeltik, Performans karşılaştırma, Kontrollü sınıflama algoritmaları

**Öz:** Asya' da bulunan birçok ülkede olduğu gibi Türkiye' de de çeltik esansiyel bitkilerden biri olup, tava üretim sistemleri insan beslenmesinden çevresel perspektifte bir çok süreç için kilit role sahiptir. Bu nedenle, üretim alanlarının belirlenmesi farklı disiplinlerden birçok araştırmacı, planlayıcı ve karar vericiler yönünden hala önemli bir konu teşkil etmektedir. Çalışmada Çanakkale ili Biga ilçesinde konumlanan karışık üretim alanların içerisindeki çeltik alanlarının belirlenmesinde en çok kullanılan sınıflama algoritmaları arasından en büyük olabilirlik (ML), rastsal orman (RF) ve k-en yakın komşu (KNN)' nun performans değerlendirilmesi amaçlanmıştır. 04 Haziran 2022 tarihinde çekilen Landsat 9 görüntüsünün görünür, yakın kızılötesi ve kısa dalgaboylu kızılötesi bantlarından yararlanılmıştır. Sınıflama, yoğun vejetasyon (D), seyrek vejetasyon (S), tarım alanları (A), su yüzeyi (W), yerleşim alanı – çıplak toprak (RB) ve çeltik (PR) olmak üzere 6 sınıfı içermektedir. Performanslar, aynı eğitim örnekleri ve aynı doğruluk kontrol noktaları ile test edilmiştir. Her bir sınıflamanın güvenilirliği doğruluk analizleri ile 150 rastgele eşit dağılımlı noktanın kontrolü ile yapılmıştır. Buna göre RF algoritması çeltik alanlarını %96.0' nın üzerinde doğrulukla ve ardından gelen KNN ise %92.0 doğrulukla belirleyebilmiştir. PR alanlarının yüksek doğrulukta belirlenmesinde tek tarihli Landsat 9 görüntüsünün kullanım potansiyeli olduğu görülmüştür. Sonuç olarak, benzer iklim, toprak ve arazi koşulları ile kıyaslanabilir ürün deseni koşulları altında PR alanlarının komşu sınıflardan güvenilir şekilde ayrıştırılması için RF algoritması kuvvetle önerilmekte olup, ücretsiz olması sebebiyle benzer çalışmalar için Landsat 9 önemli bir veri seti teşkil etmektedir.

## 1. INTRODUCTION

Paddy rice (PR) production has a vital role in food security, and it is a significant crop for over half of global population, whereby almost 20% of energy per capita sourced from rice consumption [1-3]. A great majority is growing in Asian countries, and the produced amount corresponds to 80% of world's total production and consumption rates [4-5]. However, many countries import rice due to their supply amount is not sufficient to meet the demands of the living population [6]. As it was cited by Semerci and Everest [7], rice production meets 80% of rice demand in Türkiye according to latest reports, whereby the gaps in the supply is met by import of approximately 150 thousand tons. Thence, prediction of rice production before harvest became an important point for forecasting the gap between production and expected consumption. On the other hand, identification of paddy rice cultivation areas is not important only in terms of nutrition or economic views, but also for controlling cropping system related environmental issues. The primary effect of paddy rice cultivation on the environment comprises from the large amount of irrigation water requirement since it is the main water intensive crop, and reported to consume almost one-fourth of world's freshwater resources [8]. In another point of view, it is one of the major contributors of anthropogenic greenhouse gas emissions, in particular, methane, whereby it is declared to be responsible for the 11% of methane emissions [9]. Therefore, up-to-date and reliable monitoring of rice planting areas has great importance in policies of food and environmental sustainability. In this context, remotely sensing data provides rapid, accurate, and relatively economic analysis of rice plantation.

Several studies have been conducted for paddy rice determination starting from 80s through different sensors, ranging from Landsat series to synthetic aperture radar data. Different techniques have developed for PR mapping in different regions of the world including particularly Asia [10], Mediterranean countries [11] and Australia [12], within the last decades [13]. Recent studies have dealt with comparison of varietal machine learning algorithms for classification of various LULC classes, as well as PR [14]. For instance, Mishra et al. [15] used knowledge-based decision tree approach, Onojeghuo et al. [16] considered support vector machines (SVM) and random forest (RF) algorithms, and Karkee et al. [17] utilized artificial neural networks. Present study focused on evaluation of different classification algorithms for paddy rice distinction using Landsat 9 imagery. Performances of three most widely used algorithms; maximum likelihood (ML), RF, and k-nearest neighborhood (KNN) were evaluated in the test site located within Biga District of Çanakkale Province, Türkiye. Although there are studies on comparison of different classifiers in the literature for different LULC types or a specific crop, they mostly based on at least a set of imageries or time series that covering different phenological stages of plants. However, it usually presents a limitation for many Landsat-based studies due to relatively low temporal resolution, whereas cloud cover may reduce the number of imageries within the growing season. Therefore, the study aimed to compare the performances of ML, RF and KNN algorithms, and investigate the potential of using one-date Landsat 9 imagery instead of multi-temporal imageries acquired in certain intervals during the growth period, for distinction of PR from other land use/land cover (LULC) classes. . To achieve this aim, the area was separated into six main LULC class including PR, the same training samples from each class were used in ML, RF, and classification steps, and accuracy of the same reference points were controlled to ensure that different performances are sourced from the properties of used algorithms.

## 2. MATERIAL AND METHOD

### 2.1. Study Area

The study was conducted within the specified area in Biga District of Çanakkale Province (40°20'12'' N - 27°17'24'' E). Figure 1 represents the location of the study area within Biga, Çanakkale and Türkiye. The 2021 year reports of Turkish Statistical Institute have revealed that Çanakkale Province includes 9.35% of Türkiye' s paddy rice cultivation areas with 121091 hectares (ha), while Biga takes the first place among 12 districts with 96341 ha, corresponding to 79.7% of whole province paddy rice areas [18]. The specified area was selected due to its complex surface properties, which represents a mixture of different LULC types that can give similar signatures with each other especially for irrigated fields, and covers an area of approximately 16380 ha.

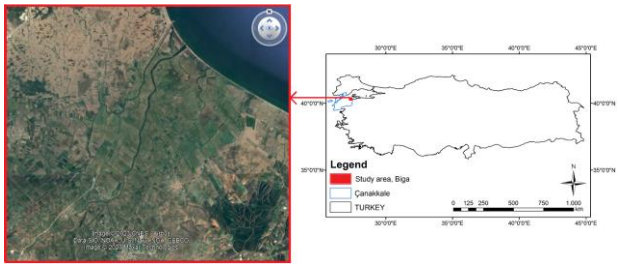


**Figure 1.** Location of study area

### 2.2. Data Collection, Image Processing, and Supervised Classification

Landsat 9 imagery has 11 bands covering different channels in between visible and thermal infrared regions of electromagnetic spectrum. Even though the band properties of Landsat 8 and Landsat 9 are near-identical to each other, enhancements in radiometric resolution led to better identification of dark surfaces, such as; water bodies. In present study, Landsat 9 imagery acquired on 04 June, 2022 is downloaded freely from United States Geological Survey website [19], and the path/row number of the imagery is 181/32 to determine paddy rice fields in the area. Level-2 production that has been geometrically, radiometrically, and atmospherically corrected was used (UTM Zone 35). The imagery was A total of six bands (6B) visible, near-infrared and shortwave-infrared bands were stacked prior to subset of the study area.

A classification scheme was composed depending on the variations in LULC types in the specified area. Accordingly, six main LULC class determined including dense vegetation (D), sparse vegetation (S), agricultural field (A), water surface (W), residential area – base soil (RB), and paddy rice (PR). The D class was consisted of dense tree cover. The S class included all types of shrubs, bushes, and harvested crop residues. The A class covered all types of agricultural production fields, except paddy rice. The W class represents water surfaces of sea or stream or open channels. The RB class covered residential areas together with bare lands, which were spectrally similar. The PR class includes the paddy rice within the specified area.

Training sample polygons from each LULC class were collected manually for the classification process depending on visual interpretation of high-resolution images from closest date of Google Earth. Supervised classification procedures were applied using three different algorithms of ML [20], RF [21], and KNN [22]. The ML algorithm calculates the likelihood allocations of classes [23]. The RF known to be a common machine learning algorithm for classification studies [24], and it's capable of increasing classification accuracy by creating multiple decision trees. The KNN classifies the unknown data by finding K-closest data from the image with the help of Euclidean distance [25]. Different parameters have tested and the most appropriate LULC maps were selected to be exposed to accuracy assessment procedures.

### 2.3. Accuracy Assessment

Finally, accuracy assessments were conducted subsequent to image classification to evaluate reliabilities of the LULC maps ($LULC_{ML}$, $LULC_{RF}$, and $LULC_{KNN}$). High-resolution Google Earth imagery with closest date was used as the reference image. In this process, accuracies of 150 randomized control points, with 25 points for each LULC class were assessed by transferring on Google Earth application (Figure 2). The well-known measures for accuracy assessment, overall accuracy (OA, %) (1), overall kappa (K) coefficient ( 2), user's accuracy (UA, %) (3), and producer's accuracy (PA, %) (4), that obtained from error matrices were evaluated for each LULC map to state the classification performances of considered algorithms. The methodological workflow is given in Figure 3.

$$OA = \frac{\sum NoCC_P}{\sum NoR_P} \times 100 \quad (1)$$

$$UA = \frac{\sum NoCC_{PLULC}}{\sum NoR_{PLULC}} \times 100 \quad (2)$$

$$PA = \frac{\sum NoCC_P}{\sum NoC_{PLULC}} \times 100 \quad (3)$$

$$K = \frac{P_0 - P_C}{1 - P_C} \quad (4)$$

Where, $\Sigma NoCC_P$ represents total number of correctly classified pixels, $\Sigma NoR_P$ total number of reference pixels, $\Sigma NoCC_{PLULC}$ total number of correctly classified pixels in a certain LULC class, $\Sigma NoR_{PLULC}$ total number of reference pixels in the same class, $\Sigma NoC_{PLULC}$ total number of classified pixels in the same class, $P_O$ probability of correct classification, $P_C$ probability of change agreement.

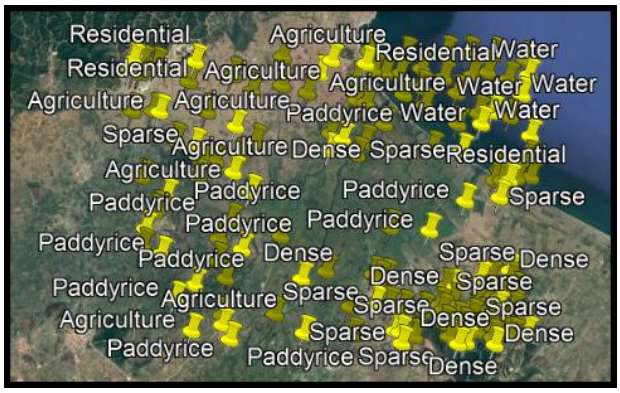


**Figure 2.** Distribution of accuracy check points

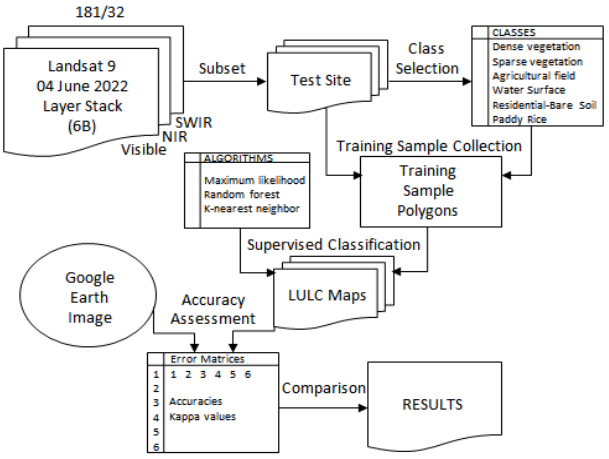


**Figure 3.** Flowchart for the supervise classification and performance comparison

## 3. RESULTS AND DISCUSSION

### 3.1. LULC Classifications

Classification of LULC is known to be one of the most widely used analyses within the frame of remote sensing, whereas Landsat imageries have long been used in several studies particularly for identification of various plants [26]. One of the main challenges for obtaining confidential LULC maps is the duration of processing time especially dealing with medium resolution imageries likewise Landsat series, which are available free of charge [27-28]. The produced maps of $LULC_{ML}$, $LULC_{RF}$, $LULC_{KNN}$ are given in Figure 4, Figure 5, and Figure 6, respectively. Areas of the LULC classes were calculated in hectares (ha) and percentages (%) (Table 1), and compared to each other. Accordingly, the area was predominantly covered by A and PR class in all classifications, whereby total area of mentioned classes corresponds to at least 55% of whole study area. Furthermore, water surface area differed slightly due to discrimination capabilities of considered algorithms for

the limited number of wet pixels on stream lines. Depending on $LULC_{ML}$, A areas seemed to cover major part of the area (29.3%), and it was followed by PR class (27.9%). Other vegetation types including dense and sparse vegetation were found as 3.5% and 19.0%, respectively, whereby the proportion of RB class was 9.6%. In comparison with $LULC_{ML}$, investigation of the class areas obtained from $LULC_{RF}$ has shown that PR class areas were quite higher than A class areas with a difference of 6.6%. Moreover, sparse and dense vegetation coverages calculated as 20.7 and 4.3%, which were both higher than $LULC_{ML}$ classification. Conversely, classification of RB areas through RF resulted in 4% lower coverage than ML. On the other hand, the class area coverages were more consistent for $LULC_{RF}$ and $LULC_{KNN}$ when compared with $LULC_{ML}$. Based on $LULC_{KNN}$, it was seen that majority of the study area was classified as PR (31.2%), while A class has the lowest share within all classifications (24.7%). The coverage of sparse vegetation showed highest value with 22.8% among all classifications. Dense vegetation was slightly lower than $LULC_{RF}$ and calculated as (4.9%). It was denoted that most effective components of supervised classification of LULC are training samples and classifiers, as well as ancillary of supplementary datasets when they are available [29]. In present study, the same training samples were utilized for all classifications for a systematic assessment of performances by avoiding the differences sourced from use of variant datasets. Therefore, the differences between LULC maps are only resulted from the discrimination properties of different classifiers, whereby the performances were determined through accuracy assessment procedures. Visual interpretations have revealed that, the RB area was overestimated especially for $LULC_{ML}$, and led to underestimation of PR class area, as well as A class. Similar situation was seen in $LULC_{KNN}$ for the misclassifications between RB and A classes, but the PR classification seemed more accurate in comparison with $LULC_{ML}$. Conversely, the $LULC_{RF}$ gave more precise results in all LULC types. Moreover, it was noticed that there were observable confusions between S and A classes in all classifiers in different rates.

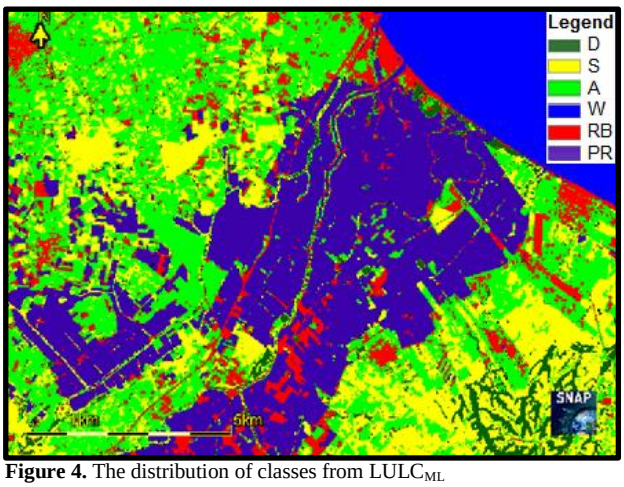


**Figure 4.** The distribution of classes from $LULC_{ML}$

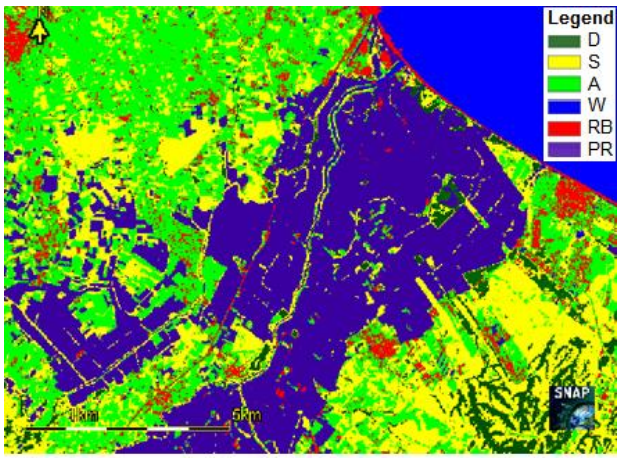


**Figure 5.** The distribution of classes from $LULC_{RF}$

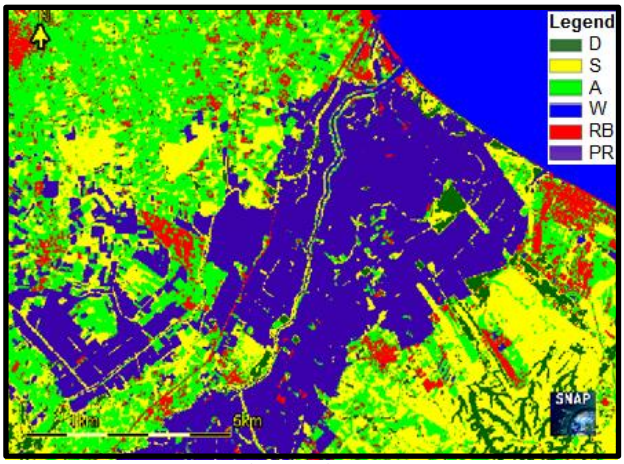


**Figure 6.** The distribution of classes from $LULC_{KNN}$



**Table 1**. Areas (ha, %) of LULC classes based on $LULC_{ML}$, $LULC_{RF}$, and $LULC_{KNN}$

| LULC CLASS | $LULC_{ML}$ | | $LULC_{RF}$ | | $LULC_{KNN}$ | |
|---|---|---|---|---|---|---|
| | Area | | Area | | Area | |
| | ha | % | ha | % | ha | % |
| D | 569.3 | 3.5 | 706.2 | 4.3 | 680.6 | 4.2 |
| S | 3106.0 | 19.0 | 3388.5 | 20.7 | 3732.3 | 22.8 |
| A | 4805.0 | 29.3 | 4265.0 | 26.0 | 4053.2 | 24.7 |
| W | 1754.6 | 10.7 | 1760.5 | 10.7 | 1768.4 | 10.8 |
| RB | 1565.5 | 9.6 | 919.3 | 5.6 | 1041.3 | 6.4 |
| PR | 4577.4 | 27.9 | 5338.3 | 32.6 | 5102.0 | 31.2 |
| Total | 16377.8 | 100.0 | 16377.8 | 100.0 | 16377.8 | 100.0 |

### 3.2. Accuracy Assessments

The performances of different algorithms were identified through accuracy assessments. Using random sampling, the randomized points from each class were distributed over the study area to guarantee the uniform and appropriate representation of the classes [30]. Determination of rice via using satellite images usually face with difficulties due to the confusions between plantations with similar color and texture [31]. The error matrices representing confusions between the classes are given in Table 2, Table 3 and Table 4 for $LULC_{ML}$, $LULC_{RF}$, and $LULC_{KNN}$ classifications, respectively. Due to the fact that the study area was composed of different types of agricultural fields, the spectral signatures were highly mixed. Furthermore, relatively small sizes of the mentioned fields were also present a handicap for the study against relatively low resolution of imagery. Thus, there were confusions between in all

LULC maps in different rates. The overall accuracies (OA) of $LULC_{ML}$, $LULC_{RF}$, and $LULC_{KNN}$ were 84.7%, 93.3% and 88.0%, respectively. Furthermore the overall kappa (OK) values were calculated as 0.816, 0.920, and 0.856 with the same order. Even though all the classifications seemed reliable since they were over the threshold kappa coefficient value, it can be clearly seen that the lowest classification performance was obtained from $LULC_{ML}$ not only for PR, but also for A classification based on the tables. The UA and PA were calculated as 80.0% and 86.9% for PR class, whereas the values were found to be 72.0% and 75.0% for A class. The confusions were occurred particularly between PR and RB class, where the water level, the height and coverage of the plants were considerably low. Moreover, there were also misclassifications in A and S classes, as well as A and RB classes. The confusions may seem relatively low due small size of study area, and thus, limited number of control points. However, greater size of test areas together with higher number of considered LULC types expected to reduce the accuracy of ML classifications in areas with similar properties.

The $LULC_{RF}$ classification gave the most reliable results for all LULC types, and accuracy indicators have shown that the distribution of classes was strongly close to real situation (93.3%). However, the most observable finding among the selected LULC types was the near-perfect classification of PR class, which was correctly classified (100%), one out of twenty six reference points was accurate, which means that and only one control point from W class was misclassified as PR. Depending on the finding, in can be confidently said that the RF can be used for PR classifications within complex areas due to considerably low error rates, which may not be significantly affected from increase of the sampling size dependent to its discrimination capability.

The investigation of error matrices for $LULC_{KNN}$ has revealed that, although the general classification were highly accurate with high OA and OK values (88.0% and 0.856), some misclassifications in PR class, in addition to low performance of classifying complex structured A class areas. Nevertheless, the use of the algorithm instead of ML is probable to give more satisfactory results in the further studies, but seemed to be less confident in comparison with RF algorithm for such purposes with 92.0 % UA and PA values for PR, and 76.0% UA and PA for A classes, respectively.

Previous studies conducted in different locations have shown that paddy rice phenology mapping is the most effective method for optical remote sensing related PR mapping with high OA [32]. Different machine learning algorithms were utilized for PR mapping, namely SVM, decision trees (DT), and RF, while advanced algorithms were also developed for obtaining classifications with higher accuracies, as it is mentioned by Zhang et al. [33] In present study, the PR determination through RF and was also prosperous with high UA and PA. In fact, as it was cited by Phan et al. [34], Mahdianpari et al. [35] and Xia et al. [36] have declared that various studies have agreed on the view of RF is considered as one of the most preferred LULC classifier over the last 20 years due to many capabilities of such as performance of higher accuracy in comparison with SVM, KNN or MLC [37-38], and rapid processing by selection of significant variables [339]. On the other hand, Zhu et al. [40] proposed a combination method consisting of phenology and machine learning approaches for determination of PR areas, and succeed with 88.8% OA, which was quite lower from the RF and KNN accuracies of present study. Furthermore, crops were identified through RF algorithm by Yao et al. [41] with OA and K values of 87.0% and 0.82, respectively, whereby the accuracies were significantly improved by combining RF and deep neural networks. In the lights of above mentioned situations, findings of the study were coherent with the literature, and believed to present a basis for further researches.

**Table 2**. Error matrix of $LULC_{ML}$

| Class | D | S | A | W | RB | PR | Total | UA (%) | PA (%) |
|---|---|---|---|---|---|---|---|---|---|
| **D** | **24** | 0 | 1 | 0 | 0 | 0 | 25 | 96.0 | 100.0 |
| **S** | 0 | **21** | 2 | 0 | 2 | 0 | 25 | 84.0 | 91.3 |
| **A** | 0 | 2 | **18** | 0 | 4 | 1 | 25 | 72.0 | 75.0 |
| **W** | 0 | 0 | 0 | **21** | 2 | 2 | 25 | 84.0 | 100.0 |
| **RB** | 0 | 0 | 2 | 0 | **23** | 0 | 25 | 92.0 | 66.1 |
| **PR** | 0 | 0 | 1 | 0 | 4 | **20** | 25 | 80.0 | 86.9 |
| **Total** | 24 | 23 | 24 | 21 | 35 | 23 | **150** | | |
| **OA** | 84.7% | | | | | | | | |
| **OK** | 0.816 | | | | | | | | |

**Table 3**. Error matrix of $LULC_{RF}$

| Class | D | S | A | W | RB | PR | Total | UA (%) | PA (%) |
|---|---|---|---|---|---|---|---|---|---|
| **D** | **24** | 0 | 1 | 0 | 0 | 0 | 25 | 96.0 | 96.0 |
| **S** | 0 | **22** | 2 | 0 | 1 | 0 | 25 | 88.0 | 96.0 |
| **A** | 1 | 1 | **20** | 0 | 3 | 0 | 25 | 80.0 | 87.0 |
| **W** | 0 | 0 | 0 | **24** | 0 | 1 | 25 | 96.0 | 100 |
| **RB** | 0 | 0 | 0 | 0 | **25** | 0 | 25 | 100.0 | 86.2 |
| **PR** | 0 | 0 | 0 | 0 | 0 | **25** | 25 | 100.0 | 96.0 |
| **Total** | 25 | 23 | 23 | 24 | 29 | 26 | **150** | | |
| **OA** | 93.3% | | | | | | | | |
| **OK** | 0.920 | | | | | | | | |

**Table 4**. Error matrix $LULC_{KNN}$

| Class | D | S | A | W | RB | PR | Total | UA (%) | PA (%) |
|---|---|---|---|---|---|---|---|---|---|
| **D** | **23** | 0 | 2 | 0 | 0 | 0 | 25 | 92.0 | 85.2 |
| **S** | 3 | **20** | 2 | 0 | 0 | 0 | 25 | 80.0 | 95.2 |
| **A** | 1 | 1 | **19** | 0 | 3 | 1 | 25 | 76.0 | 76.0 |
| **W** | 0 | 0 | 0 | **24** | 0 | 1 | 25 | 96.0 | 92.0 |
| **RB** | 0 | 0 | 2 | 0 | **23** | 0 | 25 | 92.0 | 88.5 |
| **PR** | 0 | 0 | 0 | 2 | 0 | **23** | 25 | 92.0 | 92.0 |
| **Total** | 27 | 21 | 25 | 26 | 26 | 25 | 150 | | |
| **OA** | 88.0% | | | | | | | | |
| **OK** | 0.856 | | | | | | | | |

## 4. CONCLUSIONS

Determination of PR areas has great importance in various terms, such as, yield forecast, maintenance of resources, water management, and reducing gas emissions for mitigation of climate change effects. In comparison with traditional methods, remote sensing is known to be a valuable tool for gathering information on land surface properties, whereby generation of LULC maps including different classes, comprises rapid and reliable assessment of PR areas and their effects within the concepts agricultural or environmental perspectives. On this account, along with the properties of utilized remotely sensed data; collection of training dataset, selection of appropriate classifier, and implementation of validation procedures are the most essential points of supervised classification techniques. Thereby, the major objective of present study was to compare some of the most widely used classification algorithms, namely, ML, RF, and KNN, for identifying the best performing classifier for PR detection in specified area with complex spectral structure due to spatial characteristics. Accuracy assessment procedures were conducted through the same randomized control points for $LULC_{ML}$, $LULC_{RF}$, and $LULC_{KNN}$ that collected equally from each LULC classes. Depending on the magnitude of area, a total of 150 points from the six classes were concluded to adequate and representative for evaluation of the reliability. Using the same control points in comparison step of the actual statuses with classified ones have enabled identification of best performed classification since the control points were mutual, as well as training samples, for all LULC maps. Thence, the differences between accuracies guaranteed to source from the algorithms. Findings have revealed that the most successful classification was obtained from $LULC_{RF}$ in terms of OA, K, UA, and PA with values of 93.3%, 0.920, 100.0%, and 96.0%, respectively. It was followed by KNN classifier 88.0%, 0.856, 92.0% and 92.0% with the same order, whereby the ML algorithm gave the less accurate results in all categories. The use of ML classifier in larger areas seemed probable to led reduced level of accuracy with the increment in control points and complexity level of the LULC. In present study only six LULC classes were taken into account. On the other hand, the classification scheme can be modified in different locations depending on climatic and geographic circumstances in respect to properties of land surface within the studied areas, data quality, and availability of supplementary satellite-based, aerial or ground truth data. Therefore, a further study is planned for exploring the accuracy of classification considering more LULC classes with higher number of training samples in a wider area of interest by using high-resolution datasets and derived vegetation indices. In conclusion, findings of the study findings believed to serve as a basis for future researchs by designating appropriate algorithm for the most recent Landsat data.

## REFERENCES


[1] Song Y, Wang Y, Mao W, Sui H, Yong L, Yang D, et al. Dietary cadmium exposure assessment among the Chinese population. PLoS ONE 2017;12:e0177978.

[2] Halder D, Saha JK, Biswas A. Accumulation of essential and non-essential trace elements in rice grain: Possible health impacts on rice consumers in West Bengal, India. Science of the Total Environment 2020;706:135944.

[3] Wei J, Cui Y, Luo W, Luo Y. Mapping paddy rice distribution and cropping intensity in China from 2014 to 2019 with Landsat images, effective flood signals, and Google Earth Engine. Remote Sensing, 2022;14:759.

[4] Muthayya JD, Sugimoto SD, Montgomery S, Maberly GF. An overview of global rice production, supply, trade, and consumption. Annals of the New York Academy of Sciences 2014;1324(1):7-14.

[5] Xia L, Zhao F, Chen J, Yu L, Lu M, Yu Q, et al. A full resolution deep learning network for paddy rice mapping using Landsat data. ISPRS Journal of Photogrammetry and Remote Sensing 2022;194:91-107.

[6] Saltık B, Genc L. Rice area determination using Landsat-based indices and land surface temperature values. International Journal of Agricultural and Biosystems Engineering 2016;10(7):462-470.

[7] Semerci A., Everest B. Econometric analysis of paddy production in Çanakkale Province. Türk Tarım ve Doğa Bilimleri Dergisi 2021;8(3):576-584.

[8] Cao J, Cai X, Tan J, Cui Y, Xie H, Liu F, et al. Mapping paddy rice using Landsat time series data in the Ganfu Plain irrigation system, Southern China, from 1988-2017. International Journal of Remote Sensing 2021;42(4):1556-1576.

[9] Smartt AD, Brye KR, Rogers CW, Norman RJ, Gbur EE, Hardke JT, et al. Previous crop and cultivar effects on methane emissions from drill-seeded, delayed-flood rice grown on a clay soil. Applied and Environmental Soil Science 2016:9542361.

[10] Dong J, Xiao X, Menarguez MA, Zhang G, Qin Y, Thau D, et al. Mapping paddy rice planting area in northeastern Asia with Landsat 8 images, phenology-based algorithm and Google Earth Engine. Remote Sensing of Environment 2016;185:142-154.

[11] Nguyen DB, Wagner W. European rice cropland mapping with Sentinel-1 data: the Mediterranean region case study. Water 2017;9:372.

[12] McCloy KR, Smith FR, Robinson MR. Monitoring rice areas using Landsat MSS data. International Journal of Remote Sensing 1987;8:741-749.

[13] Thorp KR, Drajat D. Deep machine learning with Sentinel satellite data to map paddy rice production stages across West Java, Indonesia. Remote Sensing of Environment 2021;265:112679.

[14] Basheer S, Wang X, Farooque AA, Nawaz RA, Liu K, Adekanmbi T, et al. Comparison of land use

land cover classifiers using different satellite imagery and machine learning techniques. Remote Sensing 2022;14:4978.
[15] Mishra VN, Prasad R, Kumar P, Srivastava PK, Rai PK. Knowledge-based decision tree approach for mapping spatial distribution of rice crop using C-band synthetic aperture radar-derived information. Journal of Applied Remote Sensing 2017;11:046003.
[16] Onojeghuo AO, Blackburn GA, Wang QM, Atkinson PM, Kindred D, Miao XY. Mapping paddy rice fields by applying machine learning algorithms to multi-temporal Sentinel-1A and Landsat data. International Journal of Remote Sensing 2018;39:1042-1067.
[17] Karkee M, Steward BL, Tang L, Aziz SA. Quantifying sub-pixel signature of paddy rice field using an artificial neural network. Computers and Electronics in Agriculture 2009;65:65-76.
[18] Turkish Statistical Institute [Internet] 2022 [Cited 2023 January 24]. Available from: https://biruni.tuik.gov.tr/medas/?locale=tr
[19] United States Geological Survey [Internet] 2022 [Cited 2022 December 16]. Available from: https://earthexplorer.usgs.gov
[20] Richards JA, Jia X. Remote sensing digital image analysis: An introduction. Berlin: Springer Verlag; 2006.
[21] Breiman, L. Random forests. Machine Learning, 2001;45(1):5-32.
[22] Fix E, Hodges JL. Discriminatory Analysis, Nonparametric Discrimination: Consistency Properties; Technique Report No. 4; U.S. Air Force School of Aviation Medicine, Randolf Field Texas: Universal City, TX, USA; 1951. p. 238-247.
[23] Erdanaev E, Kappas M, Wyss D. The identification of irrigated crop types using support vector machine, random forest and maximum likelihood classification methods with Sentinel-2 data in 2018: Tashkent Province, Uzbekistan. International Journal of Geoinformatics, 2022;18(2):37-53.
[24] Berhane TM, Lane CR, Wu Q, Autrey BC, Anenkhonov OA, Chepinoga VV, et al. Decision-tree, rule-based, and random forest classification of high-resolution multispectral imagery for wetland mapping and inventory. Remote sensing 2018;10(4):580.
[25] Kalpana YB, Nandhagopal SM. LULC image classifications using k-means clustering and knn algorithm. Dynamic Systems and Applications 2021;30(10):1640-1652.
[26] Hedayati A, Mohammad HV, Behzadi S. Paddy lands detection using Landsat-8 satellite images and object-based classification in Rasht city, Iran. The Egyptian Journal of Remote Sensing and Space Science 2022;25(1):73-84.
[27] Gomez C, White JC, Wulder AA. Optical remotely sensed time series data for land cover classification: A review. ISPRS Journal of Photogrammetry and Remote Sensing 2016;116:55-72.
[28] Yuh YG, Tracz W, Matthews HD, Turner SE. (Application of machine learning approaches for land cover monitoring in northern Cameroon. Ecological Informatics, 2023;74:101955.
[29] Johnson B. Scale issues related to the accuracy assessment of land use/land cover maps produced using multi-resolution data: Comments on "The improvement of land cover classification by thermal remote sensing". Remote Sensing 2015, 7, 8368-8390. Remote Sensing 2015;7:13436-13439.
[30] Zhao Y, Gong P, Yu L, Hu L, Li X, Li C, et al. Towards a common validation sample set for global land-cover mapping. International Journal of Remote Sensing, 2014;35:4795-4814.
[31] Abdi-Sukmono A. Identification of rice field using multi-temporal NDVI and PCA method on Landsat 8 (Case Study: Demak, Central Java). IOP Conf. Ser.:Earth and Environmental Science 2017;54:012001.
[32] Zhao R, Li Y, Ma M. Mapping Paddy Rice with Satellite Remote Sensing: A Review. Sustainability 2021;13:503.
[33] Zhang M, Lin H, Wang G, Sun H, Fu J. Mapping paddy rice using a convolutional neural network (CNN) with Landsat 8 datasets in the Dongting Lake Area, China. International Remote Sensing, 2018;10:1840.
[34] Phan TN, Kuch V, Lehnert LW. Land cover classification using Google Earth Engine and random forest classifier - the role of image composition. Remote Sensing 2020;12:2411.
[35] Mahdianpari M, Salehi B, Mohammadimanesh F, Motagh M. Random forest wetland classification using ALOS-2 L-band, RADARSAT-2 C-band and TerraSAR-X imagery. ISPRS Journal of Photogrammetry and Remote Sensing 2017;130:13-31.
[36] Xia J, Falco N, Benediktsson JA, Du P, Chanussot J. Hyperspectral image classification with rotation random forest via KPCA. IEEE Journal of Selected Topics in Applied Earth Observations and Remote Sensing 2017;10(4): 1601-1609.
[37] Rodriguez-Galiano VF, Chica-Rivas M. Evaluation of different machine learning methods for land cover mapping of a Mediterranean area using multi-seasonal Landsat images and Digital Terrain Models. International Journal of Digital Earth 2012;7:492-509.
[38] Abdel-Rahman EM, Mutanga O, Adam E, Ismail R. Detecting Sirex noctilio grey-attacked and lightning-struck pine trees using airborne hyperspectral data, random forest and support vector machines classifiers. ISPRS Journal of Photogrammetry and Remote Sensing 2014;88:48-59.
[39] Van-Beijma S, Comber A, Lamb A. Random forest classification of salt marsh vegetation habitats using quad-polarimetric airborne SAR, elevation and optical RS data. Remote Sensing of the Environment 2014;149:118-129.
[40] Zhu A-X, Zhau F-X, Pan H-B, Liu J-Z. Mapping rice paddy distribution using remote sensing by coupling deep learning with phenological characteristics. Remote Sensing 2021;13(7):1360.

[41] Yao J, Wu J, Xiao J, Zhang Z, Li J. The Classification Method Study of Crops Remote Sensing with Deep Learning, Machine Learning, and Google Earth Engine. Remote Sensing, 2022;14:2758.